Journal of Applied Polymer Science

Form birefringence and turbidity of polystyrene/poly(methyl methacrylate) blends in slit dies and planar contractions

Jorge Silva, Sebastião V. Canevarolo
Department of Materials Engineering, Federal University of São Carlos, São Paulo 13565-905, Brazil
Correspondence to: J. Silva (E-mail: jorge.silva@ufscar.br)

ABSTRACT: The birefringence and turbidity of a polystyrene/poly(methyl methacrylate) (PMMA) blend, with the concentration of the PMMA dispersed phase ranging up to 1%, were measured in both a slit channel with a constant cross section and a planar hyperbolic contraction/expansion (8:1:8). The measurements were performed by the attachment of a modular rheo-optical die to a twin-screw extruder. The optical arrangement had a red light-emitting diode as the source and two photoresistors, with one of them measuring the turbidity and the other one measuring the transmitted intensity between cross-polarizers. The experimental procedure consisted of the stopping of the extruder feeding, while the screw rotation was kept constant. Because the form birefringence could be associated with the shape of the droplets, these measurements were used to infer information about the PMMA droplet deformation and breakup. © 2016 Wiley Periodicals, Inc. J. Appl. Polym. Sci. **2016**, *133*, 44066.

KEYWORDS: blends; extrusion; morphology; polystyrene; rheology

Received 22 March 2016; accepted 6 June 2016
DOI: 10.1002/app.44066

INTRODUCTION

Subjecting a polymer blend to flow can strongly affect its microstructure. One approach to study this microstructure involves stopping the flow and quickly quenching the sample for subsequent analysis. This procedure is time expensive because it requires sample preparation, and moreover, during quenching, some relaxation of the morphology can occur. Alternatively, various techniques have been proposed to follow in real time the evolution in the microstructure of polymer blends: rheology,[1–4] dielectric spectroscopy,[5,6] small-angle light scattering,[7,8] and linear dichroism ($\Delta n''$).[9,10]

The light extinction (turbidity) has also been used to track inline the deformation and relaxation of the second phase of a polymer blend.[11,12] Zborowski and Canevarolo[12] measured the turbidity during continuous extrusion and controlled die-head pressure discharge. With blends with different viscosity ratios, they observed a high and reversible deformation in the blend having a viscosity ratio close to 1, whereas for high viscosity ratios and high matrix elasticity, a hysteresis, after an increase and subsequent decrease of the die-head pressure, was detected.

Recently, we[13] measured the birefringence and pressure drop of a polystyrene (PS) flowing through a rheo-optical slit die attached to an extruder. In that study, an innovative extruder feeding procedure was developed; this proved to be very useful because down to relatively lower values of pressure drop, the ratio between that quantity and the birefringence was achieved to be independent of the initial feeding rates.

In this study, we aimed to show that the form birefringence could be measured in diluted polymer blends to provide valuable information about the deformation and relaxation of the second phase. The turbidity and form birefringence of PS/poly (methyl methacrylate) (PMMA) blends with different concentrations were measured in a slit die with both a constant cross section and a planar contraction/expansion. To perform these measurements, a new rheo-optical die, which was an enhanced version of a previous one,[13] was designed and built, and a new optical arrangement was mounted. Because a flowing polymer blend is a complex system with several optical phenomena occurring simultaneously (light scattering, flow birefringence, form birefringence, $\Delta n''$, and Raman scattering), we revisit optical theory in this article.

EXPERIMENTAL

Materials and Blend Preparation

A commercial grade of PS, referred to as N2560, from Innova, and a PMMA, provided by Unigel, were used to prepare the PS/PMMA bends. To ensure a good dispersion and distribution and, therefore, a stable optical signal, the blends were extruded twice, with the optical signals being measured in the second extrusion only. The concentration of the PMMA dispersed phase was varied between 0 and 1% w/w.

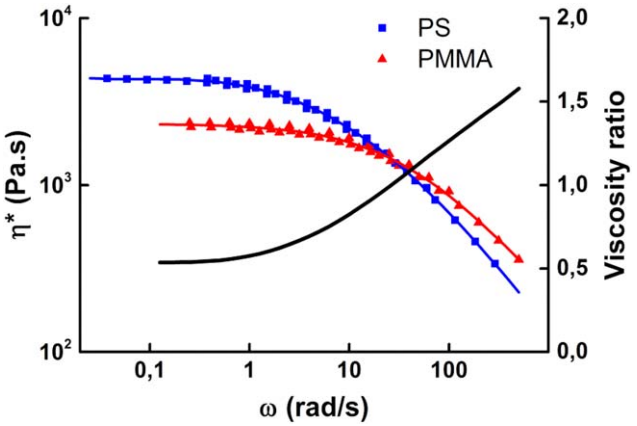

Figure 1. Complex viscosity (η^*) of PS and PMMA at 220 °C and corresponding viscosity ratio as a function of the angular frequency (ω). [Color figure can be viewed in the online issue, which is available at wileyonlinelibrary.com.]

To determine the viscosity ratio of the PS/PMMA blend and its dependence on the shear rate, rheological measurements were carried out on a rotational rheometer (ARES) equipped with parallel plates 25 mm in diameter. For each material, the experiments were conducted at three different temperatures (200, 230, and 260 °C for PS and 200, 220, and 240 °C for PMMA) under a nitrogen atmosphere to preclude or at least severely delay the oxidative degradation of the samples. The distance between the plates was set to 1 mm. The time–temperature superposition principle was assumed. The complex viscosity of the blends components and the corresponding viscosity ratio are shown in Figure 1.

For the calculation of the average droplet deformation, the values of the refractive indices of PS and PMMA were taken to be 1.59 and 1.49 (see, e.g., Oosterlinck *et al.*[14]).

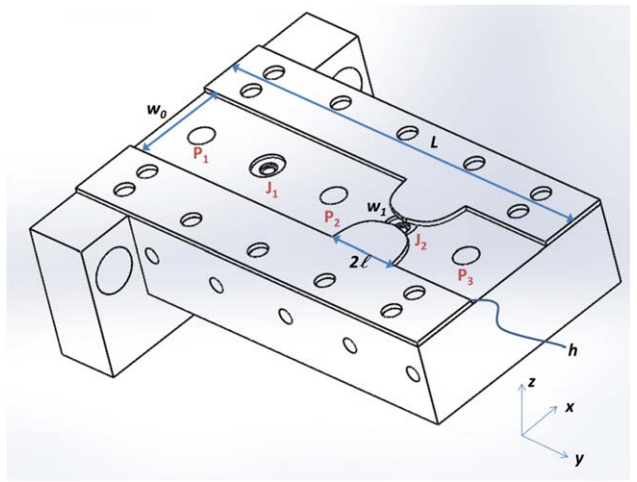

Figure 2. Bottom part of the rheo-optical die with a pair of calibrated spacers forming a channel with a planar contraction/expansion. The circles labeled P_1, P_2, and P_3 indicate the pressure transducers ports; J_1 and J_2 are the optical windows. The dimensions are as follows: w_0 = 30 mm, w_1 = 3.75 mm, L = 138 mm, 2ℓ = 24 mm, and h = 1.5 mm. [Color figure can be viewed in the online issue, which is available at wileyonlinelibrary.com.]

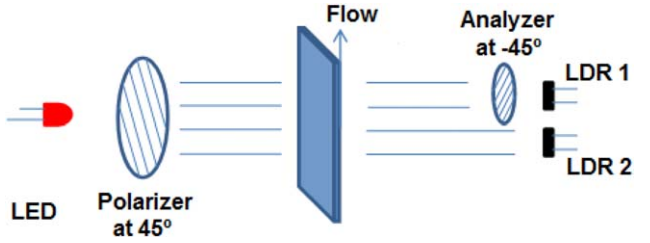

Figure 3. Schematic of the optical arrangement used in this study. [Color figure can be viewed in the online issue, which is available at wileyonlinelibrary.com.]

Experimental Apparatus

A rheo-optical die, which was an improved version of the one described in a previous work,[13] was coupled to the end of a twin-screw extruder. In short, it was composed of two modules separated by calibrated spacers that could be changed to create ducts of different widths and heights. Hence, the flow in the slit channels with different aspect ratios or even convergent or divergent channels could be studied. In this rheo-optical die, a channel width up to 30 mm was allowed, whereas in the presented in Silva *et al.*,[13] it could not exceed 10 mm. Thus, in the new die, it was possible for us to install planar contractions/expansions with higher contraction/expansion ratios without going beyond the pressure and extruder torque limits.

The length of this new die was 138 mm. The pressure transducers were located at 17.5, 71.0, and 124.5 mm from the exit, and the two optical windows were located at 44.25 and 97.75 mm. Two channel profiles were implemented. One of them had a constant cross section (width = 30 mm, height = 1.5 mm, width/height ratio = 20), and the other one had a hyperbolic contraction/expansion, as sketched in Figure 2.

The temperature control was also improved in this new rheo-optical die. The temperature of the die was now independently controlled in two zones. The first zone, which was attached to the extruder conic die, and the second one, downstream, was heated by six and four cartridge heaters, respectively. The temperature of each zone was measured with a J-type thermocouple placed at the vicinity of the channel.

The optical setup used here was the result of a modification of a previous one described in Silva *et al.*[13] In fact, with that optical arrangement, it was not possible to determine the birefringence when a significant amount of light was scattered or absorbed by the flowing material. In this study, the turbidity and transmitted light intensity between the cross-polarizers were measured simultaneously at the same optical window; this allowed the determination of the birefringence by subtraction of the effect of the turbidity from the transmitted light intensity between the cross-polarizers. The optical arrangement (Figure 3) was mounted on the transparent windows of the slit die. The light emitted by a red light-emitting diode (LED; wavelength = 620–645 nm) was polarized by a polarized filter fixed at 45° relatively to the flow direction; it reached the flowing melt material, traveled through it, and then reached two photoresistors. The first one received the light beam directly from the sample, whereas the second one was preceded by an analyzer that was mounted crosswise to the polarizer.

Experimental Procedure and Signal Analysis

The extruder was fed at constant feeding rates of 3 and 5 kg/h. The barrel temperature was set to 220 °C, and the screw speed was kept constant at 100 rpm. In the steady state, the data of the pressure transducers and photoresistors were recorded, and thereafter, the feeding was stopped (the cessation of extruder feeding) while the data were still recorded and the screw still rotated at the same constant speed.

THEORY

The study of plane–wave propagation in absorbing anisotropic media requires a substitution of the real refractive index with the complex refractive index (n^*). In analogy with isotropic media, we can write the following:

$$\begin{aligned} n^*_{xx} &= n'_{xx} + in''_{xx} \\ n^*_{yy} &= n'_{yy} + in''_{yy} \end{aligned} \tag{1}$$

where n' and n'' are the propagation and attenuation refractive indices, respectively, and i is the imaginary unit. The directions of the principal axes of the two tensors coincide.

If the flowing material in Figure 2 is coaxially birefringent/dichroic oriented at 0° with the flow direction, the Mueller matrices formalism can be used to calculate the cross-polarized transmitted light intensity measured by the photoresistor [light-dependent resistor (LDR) 1] that is placed behind the analyzer.[15] The unpolarized wave issued from the source with intensity I_0 is described by the Stokes vector $\mathbf{S_0}$. The polarizer and analyzer are described by the Mueller matrices $\mathbf{M_P}$ and $\mathbf{M_A}$, respectively, whereas, the effect of the flowing material is given by $\mathbf{M_S}$. Thus, the polarization state of the wave reaching the photoresistor LDR 1 is represented by the vector $\mathbf{S_1}$[16]:

$$S_1 = M_A \times M_S \times M_P \times S_0$$

$$S_1 = \begin{pmatrix} 1 & \cos 2\phi & \sin 2\phi & 0 \\ \cos 2\phi & \cos^2 2\phi & \sin 2\phi \cos 2\phi & 0 \\ \sin 2\phi & \sin 2\phi \cos 2\phi & \sin^2 2\phi & 0 \\ 0 & 0 & 0 & 0 \end{pmatrix}$$

$$\times \frac{1}{2}.\exp\left(-\frac{2\pi(n''_{yy}+n''_{xx})d}{\lambda}\right).\begin{pmatrix} \cosh\delta'' & -\sinh\delta'' & 0 & 0 \\ -\sinh\delta'' & \cosh\delta'' & 0 & 0 \\ 0 & 0 & \cos\delta' & \sin\delta' \\ 0 & 0 & -\sin\delta' & \cos\delta' \end{pmatrix}$$

$$\times \begin{pmatrix} 1 & \cos 2\theta & \sin 2\theta & 0 \\ \cos 2\theta & \cos^2 2\theta & \sin 2\theta \cos 2\theta & 0 \\ \sin 2\theta & \sin 2\theta \cos 2\theta & \sin^2 2\theta & 0 \\ 0 & 0 & 0 & 0 \end{pmatrix} \times \begin{pmatrix} I_0 \\ 0 \\ 0 \\ 0 \end{pmatrix} \tag{2}$$

where ϕ and θ are the angles between the flow direction and the transmission axes of the analyzer and polarizer, respectively, that is, 45 and −45°, and δ' and δ'' are the retardation and extinction, respectively. They are defined as follows:

$$\delta' = \frac{2\pi(n'_{yy}-n'_{xx})d}{\lambda} \tag{3}$$

$$\delta'' = \frac{2\pi(n''_{yy}-n''_{xx})d}{\lambda} \tag{4}$$

with d is the optical path and λ is the wavelength. The intensity I_1 is given by the first element of $\mathbf{S_1}$:

$$I_1 = \frac{I_0}{4}.\exp\left(-\frac{2\pi(n''_{yy}+n''_{xx})d}{\lambda}\right)[\cosh\delta'' - \cos\delta'] \tag{5}$$

Obviously, the term $\exp[-2\pi(n''_{yy} + n''_{xx})d/\lambda]$ is associated with scattering and absorption and can be determined with data measured by LDR 2 (Figure 2).

For the light traveling until photoresistor LDR 2, the Stokes vector $\mathbf{S_2}$ is represented by

$$S_2 = M_S \times M_P \times S_0 \tag{6}$$

This results in an intensity I_2:

$$I_2 = \frac{I_0}{2}.\exp\left(-\frac{2\pi(n''_{yy}+n''_{xx})d}{\lambda}\right)\cosh\delta'' \tag{7}$$

When I_1 is normalized with I_2, the effect of the turbidity is eliminated:

$$\frac{I_1}{I_2} = \frac{1}{2}\left(1 - \frac{\cos\delta'}{\cosh\delta''}\right) \tag{8}$$

For a constant extinction δ'', $I_1/I_2(\delta')$ becomes a sinusoidal function of the retardation. If $\Delta n''$ vanishes, that is, $\delta'' = 0$, eq. (8) reduces to:

$$\frac{I_1}{I_2} = \sin^2\left(\frac{\delta'}{2}\right) \tag{9}$$

Moreover, an analysis of eq. (8) shows that, regardless of the value of δ'', the function $I_1/I_2(\delta')$ always oscillates around 0.5. However, the amplitude of that sinusoidal wave decreases with the increase of δ''. Depending on $\Delta n''$, these reductions in the amplitude can be substantial. For blends of polyisobutene and polybutadiene or polydimethylsiloxane, at moderate and relatively high shear rates, values of $\Delta n''$ in the range 10^{-7} to 10^{-4} have been found.[9,10,17,18] The $\Delta n''$ values of PS/PMMA blends were measured by Oosterlinck *et al.*[14] during the startup of uniaxial elongational flows, with values between 10^{-6} and 10^{-5} being obtained. For example, with the largest of these values (10^{-4}) and with d and λ of the current experimental setup taken into account, $I_1/I_2(\delta')$ would have an amplitude of about 0.43. On the other hand, for $\Delta n'' = 10^{-7}$, the amplitude could be approximated as 1; that is, $\Delta n''$ could be neglected and eq. (9) could be used instead.

RESULTS AND DISCUSSION

Slit Die

It is known that the turbidity generated by a solution of particles depends on the ratio between their radii and the wavelength of incident radiation. Moreover, it was already shown in previous works that the turbidity can be sensitive to the

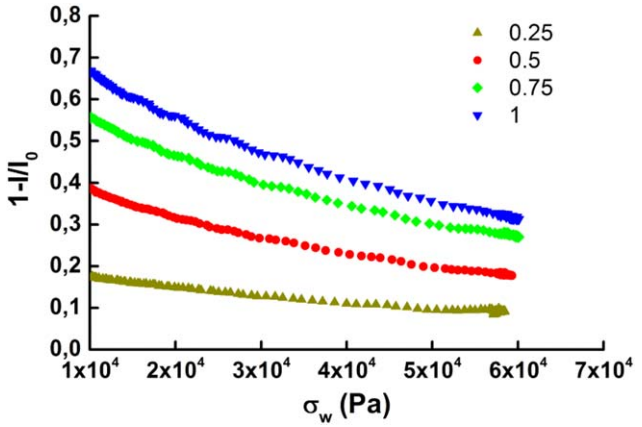

Figure 4. Turbidity as a function of stress at the wall (σ) of the PS/PMMA blends measured in the slit die at 220 °C. The data were obtained after the cessation of extruder feeding (i.e., the experimental points were obtained from right to left). The initial feeding rate was 5 kg/h. The figure caption indicates the concentrations of PMMA (% w/w). [Color figure can be viewed in the online issue, which is available at wileyonlinelibrary.com.]

concentration of the second phase in polymer blends[19–21] and to its deformation under flow.[11,12] In this study, for PS/PMMA blends, the decrease in the pressure drop after the cessation of extruder feeding was accompanied by a continuous increase in the turbidity (Figure 4). This behavior was associated with a continuous retraction of initially highly elongated droplets and/or with a continuous change in their sizes. In addition, as expected, the turbidity increased as the concentration of the PMMA dispersed phase increased when measured up to 1 wt % PMMA in PS. If the morphology of PS/PMMA is not affected by the PMMA concentration, which should be true at low concentrations, the following relation is expected to hold:[21–23]

$$\ln\left(\frac{I_0}{I}\right) = Kc \tag{10}$$

where K is a constant, I is the transmitted intensity and c is the particle concentration. In fact, a linear relation was observed in the graph of Figure 5.

At this point, it was not clear yet whether the variation of turbidity was due to droplet relaxation only or to variation in the droplet sizes during the extruder discharge. The analysis of the total birefringence data obtained from the other photoresistor (LDR 1) should give us better insight into this answer.

As was discussed previously, if the $\Delta n''$ is enough small, eq. (9) should holds, and thus, when δ' is continuously changed, the maximum of I_1/I_2 is expected to be 1. However, it was not possible to obtain reproducible results for the maximum of I_1/I_2. There were several experimental errors associated with these experiments that could have generated the nonreproducibility of the absolute values of I_1/I_2. For example, the experimental setup used real polarizer filters and did not allow accurate alignment between them. Nonetheless, the position of the maximum for the curve I_1/I_2 was highly reliable and corresponded to a d difference of λ/2. Hence, we chose to normalize the quantity I_1/I_2 such that the maximum corresponded to 1. As shown in Figure 6(a), that maximum was shifted to higher shear stresses as the concentration of the PMMA phase increased. With the assumption that $\Delta n''$ was enough small, as previously discussed, such a displacement corresponded to a decrease in birefringence (it was necessary to use a higher stress at the wall to get to the same OPD of λ/2). When the sample d (slit thickness) was known, the OPD could be converted to birefringence,[13] as shown in Figure 6(b). Differences among the birefringences of the different blends were observed for almost the entire range of measured shear stresses, from the flowing material at steady state down to the relatively low pressure drops.

A possible reason for the shift in the total birefringence measured was the contribution of the form birefringence produced by the deformed PMMA dispersed particles in the PS matrix. The flow birefringence of PS was negative:

$\Delta n_M = n_{yy,M} - n_{xx,M} < 0$ (for zero, dichroism $n_{xx,M} = n_{xx,M}^{n\prime}$ and $n_{yy,M} = n_{yy,M}^{n\prime}$)

However, cylinders and prolate ellipsoids may have generated positive-form birefringence:

$\Delta n_F = n_{yy,F} - n_{xx,F} > 0$

Hence, the birefringence of the blend (Δn_B) was given by $n_{yy,F}$:

$$|\Delta n_B| = |\Delta n_M| - |\Delta n_F| \tag{11}$$

According to the works of Wiener,[24] Bragg and Pippard,[25] and Haskell *et al.*,[26] for a diluted suspension of ellipsoids, $n_{xx,F}$ is given by

$$n_{yy,F}^2 = \frac{n_m^2\phi_m + n_e^2\phi_e/[1+(\Delta n)L_{yy}]}{\phi_m + \phi_e/[1+(\Delta n)L_{yy}]}$$
$$n_{xx,F}^2 = \frac{n_m^2\phi_m + n_e^2\phi_e/[1+(\Delta n)L_{xx}]}{\phi_m + \phi_e/[1+(\Delta n)L_{xx}]} \tag{12}$$

where ϕ_e and ϕ_m are the volume fractions of the ellipsoids and matrix, respectively; n_e and n_m are their respective refractive indices the term delta n is given by the relation $(n_e^2 - n_m^2)/n_m^2$; and L_{yy} and L_{xx} are the depolarizing factors for the parallel and perpendicular polarizations, respectively. The depolarizing factors are a function of the geometry of the droplets. Mathematical expressions that relate them with the semiaxis of an general

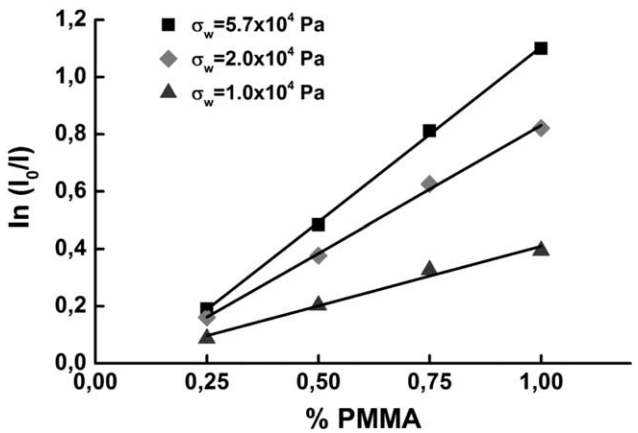

Figure 5. Normalized light extinction as a function of the PMMA concentration at different values of stress at the wall. The solid lines are linear fittings.

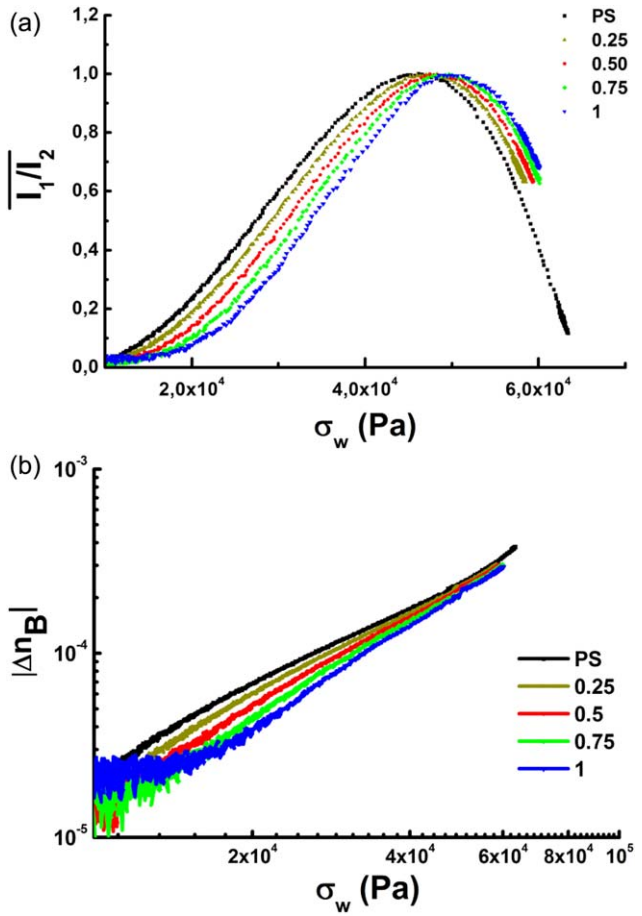

Figure 6. (a) Normalized intensity between cross-polarizers and (b) birefringence (Δn_B) as a function of stress at the wall of the PS and PS/PMMA blends measured in the slit die at 220 °C. The figure captions indicate the concentrations of PMMA (% w/w). [Color figure can be viewed in the online issue, which is available at wileyonlinelibrary.com.]

ellipsoid can be found in Osborn.[27] The sum of the three depolarizing factors equals the unit, that is

$$L_{xx} + L_{yy} + L_{zz} = 1$$

where L_{zz} is the depolarizing factor in the z direction. However, because for the optical setup assembled for this study the form birefringence was measured in the *x*–*y* plane only, it was not possible to directly deduce anything about L_{zz}. Moreover, the depolarizing factors could not be calculated from $|n_{yy,F} - n_{xx,F}|$ unless some relation between L_{yy} and L_{xx} was given. Obviously, a relation between these two variables could be established only if a particular geometry was considered. For prolate ellipsoids

$L_{yy} + 2L_{xx} = 1$ with the equation for L_{xx} and L_{yy} being[27]

$$L_{yy} = \frac{1}{m^2-1}\left[\frac{m}{2(m^2-1)^{1/2}} \times \ln\left(\frac{m+(m^2-1)^{1/2}}{m-(m^2-1)^{1/2}}\right) - 1\right] \quad (13)$$

$$L_{xx} = \frac{m}{2(m^2-1)}\left[m - \frac{1}{2(m^2-1)^{1/2}} \times \ln\left(\frac{m+(m^2-1)^{1/2}}{m-(m^2-1)^{1/2}}\right)\right]$$

where m is the droplet deformation parameter i.e., it is the ratio between the semiaxes of the ellipsoid. The limiting case of an infinitely long cylinder, $m = \infty$, leads to $L_{yy} = 0$ and $L_{xx} = 1/2$.

In this study, the deformation of ellipsoids was calculated with the assumption of a prolate ellipsoid. Although it is well known that the droplets in polymer blends do not deform necessarily as a prolate ellipsoid[28,29] (in general, the three semiaxes of the ellipsoid have different dimensions), we think that this approximation will help with the discussion of the results.

At low concentrations and for typical values of n_e and n_m, we affirmed, with just small error, that the form birefringence was proportional to the volume fraction of the dispersed phase. Thus, eq. (11) could be rewritten as follows:

$$|\Delta n_B| \cong |\Delta n_M| - \frac{d(\Delta n_F)}{d\phi_e}(\phi_e=0)\phi_e$$

$$|\Delta n_B| \cong |\Delta n_M| - \frac{(3L_{xx}-1)n_m(n_e^2-n_m^2)^2}{2[(2L_{xx}-1)n_e^2-2L_{xx}n_m^2][n_m^2+L_{xx}(n_e^2-n_m^2)]}\phi_e \quad (14)$$

Hence, at a given pressure drop, curves of $|\Delta n_B|$ versus ϕ_e should be a straight line if it is assumed that (1) the deformation of the droplets is the same for all blends and (2) the concentration of the second phase is low enough to not affect the rheology of the polymer matrix flow. The slope could be used to calculate m with eqs. (13) and (14). In this study, the m parameter was calculated by numerical methods with Wolfram Mathematica software.

Figure 7(a) shows that for a given shear stress, the birefringence varied linearly with the volume fraction of PMMA; this was in good agreement with the previous discussion. Data of PS were not used in this calculation because this material was not subjected to the same processing history as the blends. The ratio between the axes of a prolate ellipsoid (m), calculated from the slopes of Figure 7(a), are shown in Figure 7(b). As the shear stresses decreased after the cessation of extruder feeding, the deformation of the droplets seemed to increase slightly until to reach a maximum around 30 kPa before completely relaxing to 1. At first sight, these data were at odds with those from the turbidity (Figure 4), which indicated a progressive relaxation until a spherical shape was reached. A morphological picture that explained these results was the following: even though the shear rate was decreasing, down to 30 kPa, the droplets elongated more and more in the flow direction. In fact, it is known that it may be possible to break up a droplet even when the capillary number is lower that the critical capillary number because the initial shape is not spherical. Simultaneously, the droplets relax in the vorticity direction, and this causes a continuous increase in the turbidity. Thus, the apparent contradiction would root on the failure of the prolate ellipsoid model to successful describe the experimental results. Nonetheless, some facts that can make the interpretation of the results more complex should be kept in mind. First, in the slit die, the shear stress was not constant through the height of the channel; the droplets that were closer to the wall suffered higher deformation. Second, droplets of different sizes deformed differently. Third, in the theory used here to calculate m, it is assumed that

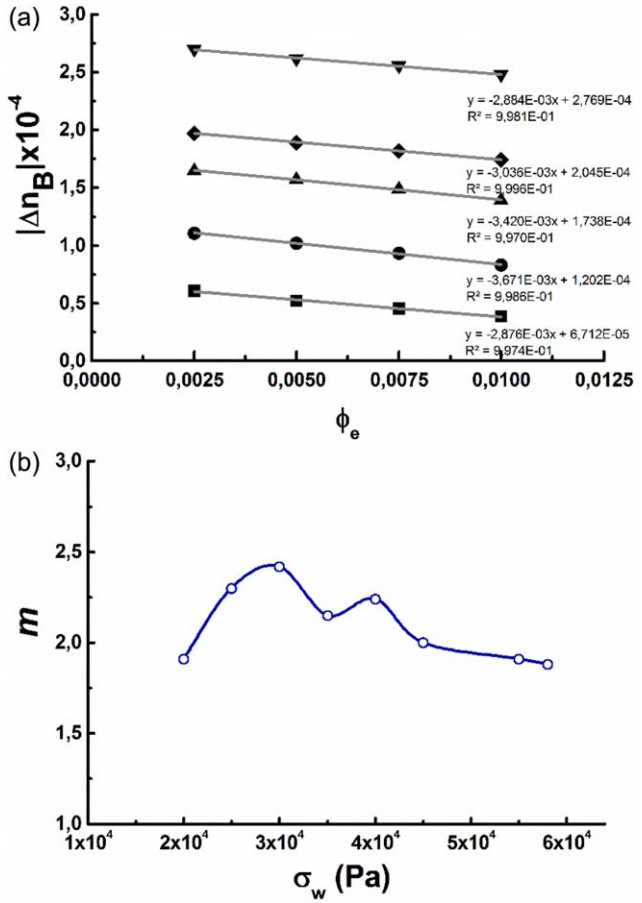

Figure 7. (a) Birefringence versus the volume fraction of PMMA at different shear stresses at the wall. A linear fit was applied to the data of each shear stress. From the bottom up, the shear stresses were 20, 30, 40, 45, and 55 kPa. (b) The ratio (m) of the axes of a prolate ellipsoid calculated with eqs. (13) and (14) as a function of the shear stresses at the wall. More slopes than those shown in panel a were determined to calculate enough points to trace the curve in panel b. [Color figure can be viewed in the online issue, which is available at wileyonlinelibrary.com.]

the droplets are aligned with the major axis in the flow direction. It is well known that, depending on the shear rate, the major axis of an ellipsoid can form a significant angle with the flow direction. Thus, the value obtained for m should be taken as an average value indicating the deformation of dispersed phase. Below 30 kPa, the birefringence results indicated droplet relaxation until a nearly isotropic shape was reached at 1 kPa.

Hyperbolic Contraction/Expansion

A similar analysis to the one performed previously was also conducted for the hyperbolic contraction/expansion die shown in Figure 2. In this case, the flow had both shear and extensional components. Furthermore, in the hyperbolic region, the cross section area was smaller than that on the slit channel, as discussed previously. Thus, for the same flow rate, higher droplet deformations were expected.

In the same way as observed for the slit die, the turbidity increased continuously as the pressure drop decreased, as shown in Figure 8. However, here, two slopes were clearly distinguishable: a lower one, extending down to about 80 MPa/m, and a higher one for lower pressure drops. The form birefringence, discussed later, supported an explanation for this variation in the slope.

The normalized cross-polarized transmitted light intensity (I_1/I_2), measured immediately after the planar contraction and before the expansion (optical window J_2), is shown in Figure 9(a). As expected, the maximum attained birefringences were much higher than those obtained in the slit die, and therefore, several orders were covered. In addition, for both the PS and the blends, two observations stood out: (1) the amplitude decreased as the pressure drop increased, and (2) the oscillation did not occur around 0.5, but rather, the medium point progressively shifted to higher values. The latter observation was due to the photoelasticity of the borosilicate windows. As the melt pressure increased, the optical windows generated a significant birefringence that added to the one of the flowing material. The former observation could, in principle, be attributed to two phenomena: $\Delta n''$ and the narrowing of the fringes in the region of measurement. As discussed previously in this article, $\Delta n''$ could have caused a decrease in the amplitude measured between the crossed polarizers. However, it was hard to conceive that it was the main thing accountable for the observed damping because that it would have required much larger values than the ones reported in the literature. In fact, the narrowing of the fringes should have been the main effect justifying the damping in the amplitude of the intensity. In fact, the measurement performed in this study was not punctual; rather, it was performed on a circle with a diameter of 3 mm. For higher pressure drops, a higher fraction of a complete fringe was in the measurement area, and therefore, lower amplitudes were measured; the brighter zone of the fringe canceled out the darker one and led the measured average intensity to an intermediate value. Interestingly, none of these phenomena should have significantly shifted the position of the maxima and minima, and thus, they were used to calculate the birefringence. In any case, when we assumed that the PS rheological behavior was not affected by

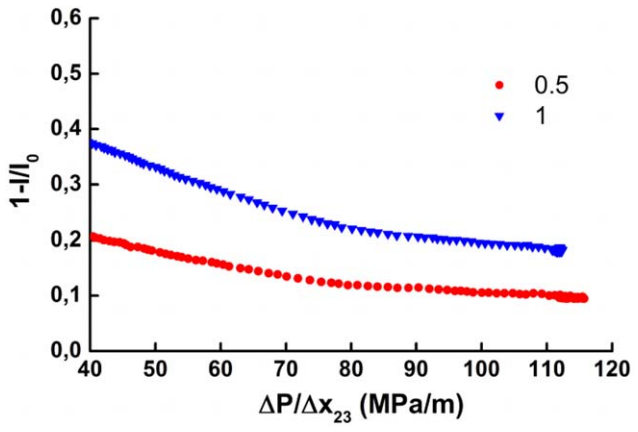

Figure 8. Turbidity as a function of the pressure drop between P2 and P3 (see Figure 2) of the PS/PMMA blends with 1 and 0.5 wt % PMMA measured in the planar convergent/divergent zone (optical window J_2) at 220 °C after the stopping of the feed from a steady-state flow of 5 kg/h. [Color figure can be viewed in the online issue, which is available at wileyonlinelibrary.com.]

the presence of the PMMA diluted phase (<1 wt %), the dislocations of the maxima and minima for the blends relatively to the matrix were assigned only to the form birefringence of the dispersed PMMA particles.

Because of the damping in the normalized intensity curves discussed later, the birefringence could only be calculated at the maximum and minimum points. The graph of Δn_Bs is shown in Figure 9(b). To be able to estimate the form birefringence and, therefore, the droplet deformation, the points obtained for each blend were fitted with a polynomial equation. The resulting deformation of a hypothetical prolate ellipsoid is shown in Figure 10. Because the form birefringence was relatively small and the number of points was reduced, there was a large uncertainty associated with m values; in fact, fitting the data of birefringence with a polynomial equation of order 3 instead of 4 led to significant changes in the calculated m. However, regardless the order of the polynomial equation used to fit the data, a maximum in the deformation parameter, occurring at about 90 MPa/m, was always observed. This large value certainly

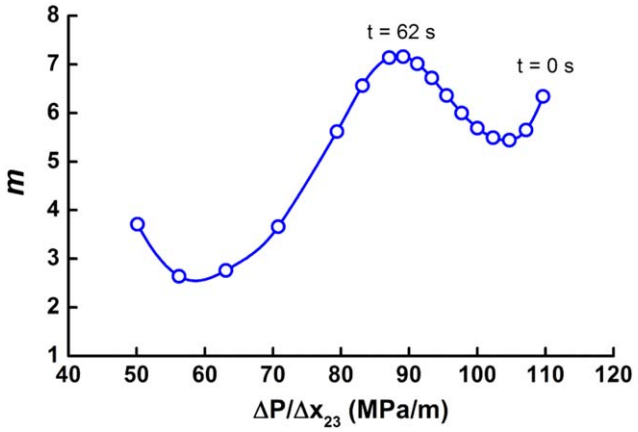

Figure 10. Ratio (m) of the axes of a prolate ellipsoid calculated with eqs. (13) and (14) as a function of the pressure drop between P2 and P3. The times, t, shown in the figure were counted from the moment at which the extruder feeding was stopped. [Color figure can be viewed in the online issue, which is available at wileyonlinelibrary.com.]

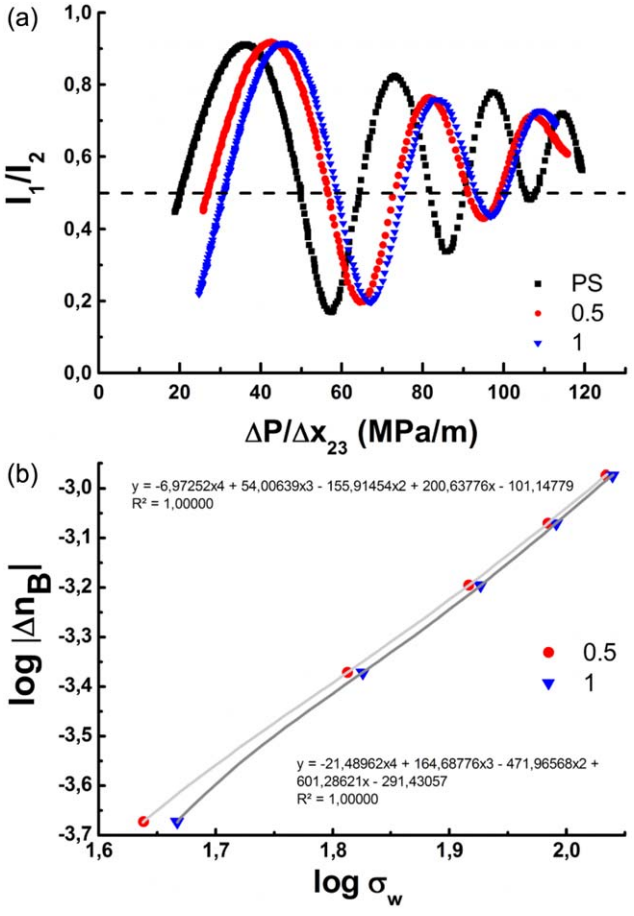

Figure 9. (a) Normalized intensity between cross-polarizers of the PS and PS/PMMA blends measured in the planar convergent/divergent zone at 220 °C. The initial feeding rate was 5 kg/h. (b) Corresponding birefringence of the blends as calculated in the maxima and minima fitted by a fourth-order polynomial equation. [Color figure can be viewed in the online issue, which is available at wileyonlinelibrary.com.]

indicated the existence of very elongated fibrils at this point of the experiment. Remember that the slope in the turbidity curves in Figure 8 changed at about 80 MPa/m; this supported the idea that the interval 80–90 MPa/m was a critical region. These results seem to indicate that for higher values of pressure drop, breakup occurred to some extent. At lower pressure drops, as the pressure drop decreased, the droplet deformation seemed to increase slightly. This behavior was similar to that described previously for the slit die with constant cross section, and therefore, the explanation should be the same.

The experiments described previously were performed in transient mode: the optical signals and pressure drops were measured after a cessation of extruder feeding, with the values of the flow rate in the die being continuously reduced. Thus, it was important to understand whether these results could be extrapolated to the steady state. The data obtained at 3 kg/h (not shown here) were coincident with those acquired after the cessation of feeding at 5 kg/h; this indicated that the extrapolation may have been valid. In fact, when compared with the typical relaxation times of the PS matrix, the timescale of the cessation of feeding experiments was large. However, because the relaxation of the dispersed phase was slower, that extrapolation should be taken with prudence.

Additional experiments are needed to confirm the propriety of the morphological evolution suggested previously to explain the experimental observations. We are now preparing light-scattering experiments to clarify the results discussed in this article.

CONCLUSIONS

An optical arrangement was installed in a modular rheo-optical die; this was attached to a twin-screw extruder, and this allowed us to simultaneously measure the turbidity and birefringence of a flowing material. In particular, the form birefringence of a PS/PMMA blend generated by the deformed droplets was

measured. As predicted, at low concentrations, the form birefringence showed a linear dependence on the PMMA content. With the assumption that the prolate ellipsoids aligned with the flow direction, an average deformation of the droplets was calculated. Even though this calculation was an approximation (the droplets did not necessarily deform in prolate ellipsoids and may not have been aligned with the flow direction), together with the turbidity, these data provided valuable information about the deformation of the particles of the second phase. The results obtained in the planar contraction/expansion flow suggest the existence of a critical pressure drop, above which the fibrils broke up to some extent.

The evolution of the morphology inferred by the analysis of the form birefringence and turbidity measured in this study still need to be confirmed by other experimental techniques. However, as far as we know, this is the first time that a measurement of the form birefringence in molten polymer blends has been reported in the literature.

ACKNOWLEDGMENTS

Financial support from Coordenação de Aperfeiçoamento de Pessoal de Nível Superior (contract grant number BJT 019/2012 to Jorge Silva) and Conselho Nacional de Desenvolvimento Científico e Tecnológico (PQ scholarship 311790/2013-5 to Sebastião V. Canevarolo) is gratefully acknowledged.

REFERENCES

1. Friedrich, C.; Gleinser, W.; Korat, E.; Maier, D.; Weese, J. *J. Rheol.* **1995**, *39*, 1411.
2. Takahashi, Y.; Kurashima, N.; Noda, I.; Doi, M. *J. Rheol.* **1994**, *38*, 699.
3. Vinckier, I.; Moldenaers, P.; Mewis, J. *J. Rheol.* **1996**, *40*, 613.
4. Vinckier, I.; Moldenaers, P.; Mewis, J. *J. Rheol.* **1997**, *41*, 705.
5. Boersma, A.; Wubbenhorst, M.; van Turnhout, J. *Macromolecules* **1997**, *30*, 2915.
6. Tajiri, K.; Ohta, K.; Nagaya, T.; Orihara, H.; Ishibashi, Y.; Doi, M.; Inoue, A. *J. Rheol.* **1997**, *41*, 335.
7. Santos, A. M. D.; Caceres, C. A.; Calixto, L. S.; Zborowski, L.; Canevarolo, S. V. *Polym. Eng. Sci.* **2014**, *54*, 386.
8. Teixeira, P. F.; Maia, J. M.; Covas, J. A.; Hilliou, L. *Polym. Test.* **2014**, *37*, 68.
9. Vermant, J.; Van Puyvelde, P.; Moldenaers, P.; Mewis, J.; Fuller, G. G. *Langmuir* **1998**, *14*, 1612.
10. Yang, H.; Zhang, H. J.; Moldenaers, P.; Mewis, J. *Polymer* **1998**, *39*, 5731.
11. Zborowski, L.; Canevarolo, S. V. *Polym. Eng. Sci.* **2013**, *53*, 2422.
12. Zborowski, L.; Canevarolo, S. V. *Polym. Test.* **2012**, *31*, 254.
13. Silva, J.; Santos, A. C.; Canevarolo, S. V. *Polym. Test.* **2015**, *41*, 63.
14. Oosterlinck, F.; Mours, M.; Laun, H. M.; Moldenaers, P. *J. Rheol.* **2005**, *49*, 897.
15. Benoit, A. M.; Naoun, K.; Louis-Dorr, V.; Mala, L.; Raspiller, A. *Appl. Opt.* **2001**, *40*, 565.
16. Fuller, G. G. Optical Rheometry of Complex Fluids; Oxford University Press: New York, **1995**.
17. Van Puyvelde, P.; Yang, H.; Mewis, J.; Moldenaers, P. *J. Colloid Interface Sci.* **1998**, *200*, 86.
18. Van Puyvelde, P.; Yang, H.; Mewis, J.; Moldenaers, P. *J. Rheol.* **2000**, *44*, 1401.
19. Melo, T. J. A.; Canevarolo, S. V. *Polym. Eng. Sci.* **2002**, *42*, 170.
20. Melo, T. J. A.; Canevarolo, S. V. *Polym. Eng. Sci.* **2005**, *45*, 11.
21. Pinheiro, L. A.; Hu, G. H.; Pessan, L. A.; Canevaro, S. V. *Polym. Eng. Sci.* **2008**, *48*, 806.
22. Meeten, G. H. Optical Properties of Polymers; Elsevier Applied Science: London, **1986**.
23. Melik, D. H.; Fogler, H. S. *J. Colloid Interface Sci.* **1983**, *92*, 161.
24. Wiener, O. H. Die Theorie des Mischkörpers für das Feld der Stationären Strömung. 1. Abhandlung: Die Mittelwertsätze für Kraft, Polarisation und Energie; B. G. Teubner: Leipzig, **1912**.
25. Bragg, W. L.; Pippard, A. B. *Acta Crystallogr.* **1953**, *6*, 865.
26. Haskell, R. C.; Carlson, F. D.; Blank, P. S. *Biophys. J.* **1989**, *56*, 401.
27. Osborn, J. A. *Phys. Rev.* **1945**, *67*, 351.
28. Jackson, N. E.; Tucker, C. L. *J. Rheol.* **2003**, *47*, 659.
29. Yu, W.; Bousmina, M. *J. Rheol.* **2003**, *47*, 1011.